The Pennsylvania State University

The Graduate School

College of Engineering

A MODEL FOR SIMULATING THE COMPRESSION STIFFNESS DEGRADATION IN CIRCULAR ELASTOMERIC BEARINGS DUE TO FATIGUE

A Thesis in

Civil Engineering

by

Pu Deng

Submitted in Partial Fulfillment
of the Requirements
for the Degree of

Master of Science

August 2013

The thesis of Pu Deng was reviewed and approved* by the following:

Gordon Warn

Assistant Professor of Civil Engineering

Thesis Adviser

Charles E. Bakis

Distinguished Professor

Maria Lopez de Murphy

Associate Professor of Civil Engineering

Peggy Johnson

Professor of Civil Engineering,

Department Head

*Signatures are on file in the Graduate School.

Table of Contents

List of Tables

List of Figures

Chapter 1

Introduction

1.1 Background and Motivation

Elastomeric bearings are widely used in civil, rail and aerospace applications to suppress vibrations. These bearings are manufactured in a variety of different shapes and configurations for various loading conditions e.g., axial, radial, multi-axial. Most elastomeric bearings consist of multiple layers of elastomer bonded to intermediate steel "shim" plates. After repeated cycles of mechanical loading, fatigue cracks will initiate at the edge of the laminate and propagate toward the interior of the bearing leading potentially to significant changes in the stiffness properties of the bearings. Past studies, e.g. Roeder et al. (1990), Chou and Huang (2008), among others, have demonstrated that fatigue induced cracking has led to reductions in compression stiffness of 18.5 and 18.9% after 2.45×10^5 and 3.38×10^5 cycles respectively. Identifying the initiation of these fatigue cracks is important in the aerospace industry for maintenance of rotorcraft and replacement of the bearing components before significant stiffness degradation occurs to prevent undesirable modes of vibration. In civil infrastructure, such as bridges, the shear strains in the elastomer under design loading are limited to a specific value (Roeder et al. 1990; AASHTO 2010) in an attempt to limit fatigue induced cracking over the design life of the bridge. According to National Bridge Inventory (NBI) (2010) the total average daily traffic of Pittsburgh, Pennsylvania (PA) in 2010 is 8,360,661 over total 720 bridges which gives average daily traffic of one bridge 11,612 meaning that for a 50 year design life elastomeric bearings supporting such a bridge would be subjected to more than 2×10^8 cycles of loading which exceeds the number reported by Roeder et al. that lead to an 18.5% degradation in stiffness. Given that the majority of bridges remain in service well beyond their intended service life suggests that elastomeric bearings are likely to be fully fatigued while in-service thereby altering the

dynamic behavior of the bridge leading to increases in service deflections and unanticipated shifts in the modal frequencies.

1.2 Objective

To date most analytical work pertaining to the fatigue of elastomeric bearings has focused on predicting the initiation of fatigue cracking (Chou and Huang 2011) to set inspection and replacement intervals for rail and aerospace components. For rail and aerospace applications the bearing component is likely to be removed prior to significant changes in stiffness, however, for bridges applications significant changes in the stiffness of the elastomeric bearings are to be expected during the design life. An understanding of the relationship between cycles of loading, crack initiation and propagation, and the resulting changes in the stiffness properties could prove useful for determining whether fatigue in elastomeric bearings adversely affects the in-service dynamic behavior or to separate benign changes in modal frequencies from those resulting from more significant structural deterioration.

1.3 Terminology

An important terminology is widely used to express the geometry of the rubber bearing called shape factor which defines as:

$$S = \frac{\text{Loaded area}}{\text{Area free to bulge}} \tag{1}$$

where the loaded area and area free to bulge of one laminate rubber layer were shown in Fig.1(a)

After cyclic loading, the vertical stiffness degradation will eventually enters a relative stabilized status when its value doesn't change significantly with subsequent cycles of loading. Define the change between initial and stabilized vertical stiffness as degradation, $D_{s,}$ and the smallest number of cycles to achieve it as fatigue life, $n_{f,}$ in Fig.1(b) to describe the fatigue behavior of cyclic loaded circular rubber

bearing. The objective of the work presented in this study is to build on previous analytical knowledge and models to develop an analytical framework to simulate compression stiffness degradation due to cycles of compressive loading in axially loaded cylindrical multi-layer laminated rubber bearings and identify its corresponding degradation D_s and fatigue life n_f when subjected to different applied load and different shape factors. A global variance based sensitivity analysis is performed with the analytical model developed in this study to identify those factors, i.e. stress range, shape factor, material properties, to which fatigue life and stiffness degradation are most sensitive.

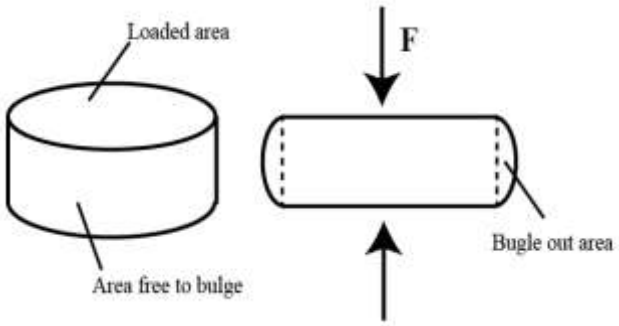

(a)

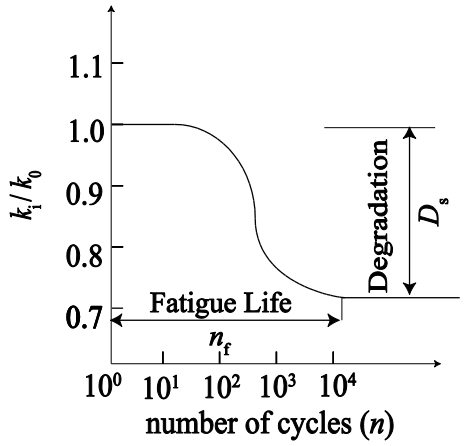

(b)

Fig.1 (a) Illustration of shape factor for on laminate of rubber layer; (b) definition of fatigue life and degradation

Chapter 2

Review of past studies

2.1 Energy release rate

The energy release rate, *G*, has been used to describe the complex rubber fatigue process. Rivlin and Thomas (1953) demonstrated that the strain energy release rate for an elastic material is:

$$G = \left(dU / dA_c \right)_l \tag{2}$$

where dU and dA_c represent per unit change of stored energy and per unit change of one crack surface area respectively. The subscript l denotes the decrease of total stored energy calculated from the specimen before and after fatigue process under the same deformation but different applied loading (Lake 2003). This concept was first proposed to investigate the material subjected to static loading but was quickly discovered also applicable for cyclic loading (Mars and Fatemi 2002). The maximum energy release rate affects the cracks growth rate, *dc/dn*, if stress ratio (minimum applied vertical stress divided by maximum applied vertical stress) equals zero (Thomas 1958).

Lake and Lindley (1966) induced a four-regime framework, illustrated in Fig. 2., to describe the relationship between the crack growth rate, *dc/dn*, and the energy release rate for rubber subjected to cyclic tension loading with a zero stress ratio. In regime 1 fatigue cracks initiate due to initial imperfections from manufacturing and propagate according to:

$$\frac{dc}{dn} = \gamma \tag{3}$$

where γ is a material parameter related to initial imperfections of the elastomer material. In regime 1, the crack growth rate, *dc/dn*, is independent of the applied force and will continue at a slow rate until the energy release rate exceeds a threshold G_0. When the energy release rate exceeds the threshold, G_0, but is below G_t, the crack growth rate enters regime 2 where the grown rate is described by:

$$\frac{dc}{dn} = A\left(G - G_0\right) \tag{4}$$

where A is a material dependent parameter that is obtained from material testing. When the energy release rate exceeds the threshold G_t, the crack growth rate enters regime 3 where the growth rate increases proportionally to G according to:

$$\frac{dc}{dn} = aG^b \tag{5}$$

where a and b are material dependent factors. When the energy release rate, G, exceeds the threshold of G_c the crack growth rate enters regime 4 in which the cracks growth becomes infinitely large. This theory gives a prototype to describe the relation between the first order derivative of fatigue cracks length, c, and number of cycles, n, when rubber is subjected to cyclic tension stress with zero stress ratio (fully relaxing).

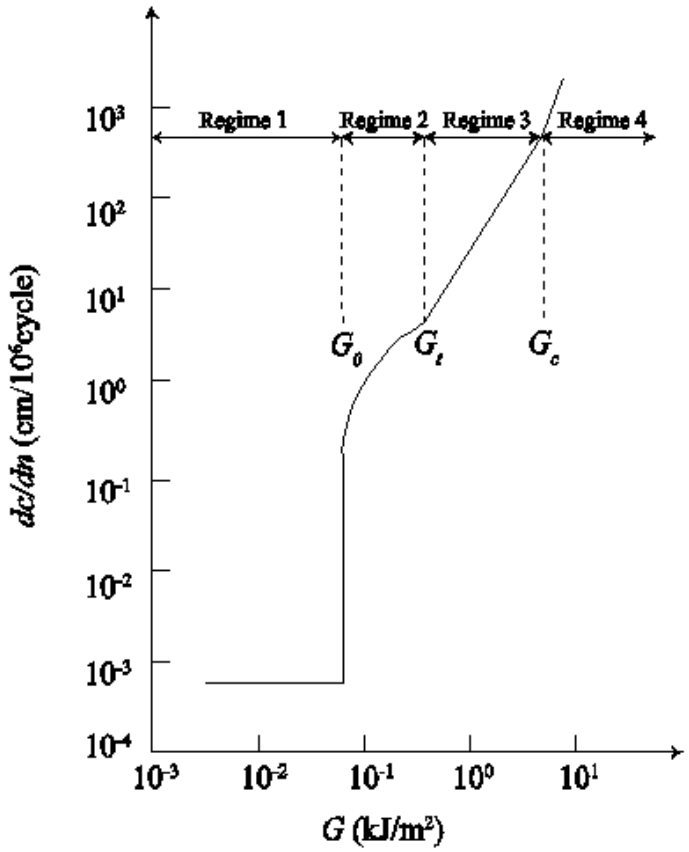

Fig. 2 Illustration of regimes for the crack growth rate as a function of the energy release rate (adopted from Chou and Huang 2012; Mars and Fatemi 2002)

2.2. Idealized cracks path

Lindley and Stevenson (1981) demonstrated that as with elastomers in tension, the relation between crack growth rate, *dc/dn*, and energy release rate, *G* is valid in compression irrespective of the specimen geometry and is an inherent material property. Lindley and Stevenson arrived at these conclusions from the results of cyclic compression tests performed on a series of bonded rubber cylinders at a specific rate to measure the *dc/dn* and calculate the energy release rate *G*, by Eq. (2). The change in stored free energy within the rubber bearing, *dU*, can be calculated from applied force and deformation of the specimen in different crack growth stages and an idealized crack path, illustrated in Fig. 3, used to calculate the change in crack surface, $A_{c,}$ according to:

$$A_c = \pi c_i \left[D - \left(D - x_1 \right) c_i / c \right] \tag{6}$$

where D is the initial diameter of bonded cylinder, x_1 is the final core diameter of the specimen after fatigue damage, c_i is the circumferential splitting crack length at one certain intermediate stages of crack growth which can be linked to the number of cycles by Eq.(2) – (5) if energy release rate G can be determined, and c is the final vertical cracks length measured from experiment.

When cracked rubber subjected to a uniaxial stress, it was found that energy release rate is affected by strain energy density, $W_{c,}$ tensile strain, ε, and the crack length, c, (Rivlin and Thomas 1953; Lindley 1972) at the cracked point which can be written as:

$$G = 2\pi(1+\varepsilon)^{-1/2} W_c c \tag{7}$$

For the multiaxial stress state (Mars, 2002) the maximum strain energy density, W_c, which is the work done by the maximum principal stresses acting on the surface of existed cracks determines the direction of the cracks and can be used to obtain the energy release rate, *G*, in Eq. (7) which in a further step determines the fatigue crack growth rate, *dc/dn*.

2.3 Stress distribution

To calculate the maximum energy density, the maximum principle stress and strain must be known. For a cylindrical elastomeric pad, a polar coordinate system can be adopted to simplify the principle stress and strain expressions (Horton et al. 2002). For a cylinder as shown in Fig.3 the stress in the radial and longitudinal coordinate axes at point (r, z) in longitudinal section θ, can be expressed as:

$$\sigma_{rr} = \sigma_{\theta\theta} = \frac{2F}{A_b}\left(1-\frac{r^2}{R^2}\right)\frac{\cosh\left[\beta\left(z-\frac{h}{2}\right)\right]}{\cosh\frac{\beta h}{2}} \tag{8}$$

$$\sigma_{zz} = \frac{F}{A_b}\left\{1+\left(1-\frac{2r^2}{R^2}\right)\frac{\cosh\left[\beta\left(z-\frac{h}{2}\right)\right]}{\cosh\frac{\beta h}{2}}\right\} \tag{9}$$

$$\sigma_{rz} = \frac{F\beta r}{6A_b}\frac{\sinh\left[\beta\left(z-\frac{h}{2}\right)\right]}{\cosh\frac{\beta h}{2}} \tag{10}$$

where F is the applied load, $A_\mathbf{b}$ is the loaded area, R is the radius of the circular bearing, $\beta=(24/R^2)^{1/2}$, and h is the total height. From Eq. (8) through (10), the principal stress σ_{p1} and σ_{p2} can be determined through a standard coordinate transformation (see Appendix-A) with which the maximum strain energy density $W_{c,}$ at cracked point in the elastomer can be determined

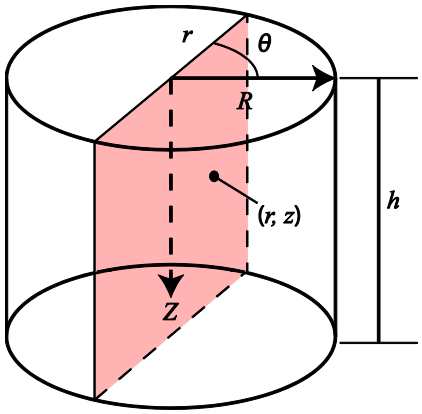

Fig. 3 Illustration of cylindrical coordinates system for a rubber cylinder

2.4 Analytical cracks trajectory

Chou and Huang (2011, 2012) proposed a second order function, z/h, to approximate the path of a fatigue crack in a longitudinal section θ of a cylindrical elastomeric pad subjected to cyclic compression, the proposed crack path equation is:

$$\frac{z}{h} = a_1\left(\frac{r}{R}\right)^2 + a_2\left(\frac{r}{R}\right) + a_3 \tag{11}$$

Where R is the radius, h is height of the rubber laminate and a_1, a_2, a_3 are coefficients determined from numerical analysis. The coefficient is dependent on the shape factor of the elastomeric layer and values proposed by Chou and Huang are presented in Table 1.

Table 1. Cracks trajectory factor values (taken from Chou and Huang 2012)

Shape Factor S	a_1	a_2	a_3	a_4^*
2.5	-72.835	135.14	-62.303	0.965667
5	-264.53	507.8	-243.27	0.982
10	-1022.6	2002.4	-979.8	0.990667
20	-3935.3	7785.1	-3849.8	0.995333

*Chou, Personal communication (August, 2012)

Note: all the values in Table 1 and Table 2 are directly from Chou and Huang (2007, 2012) and personal communication

In Table 1, a_4 (Chou, personal communication, August, 2012) limits the projection of cracks propagation on radial direction in cylindrical coordinate system as shown in Fig.4. In other words, the value of (r/R) is within the regime: a_4<(r/R)<1.

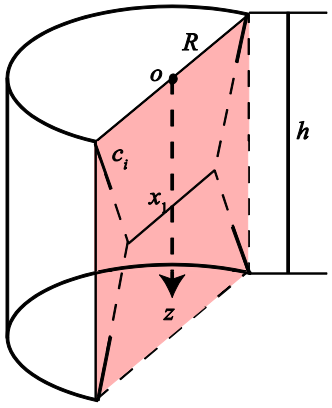

(a)

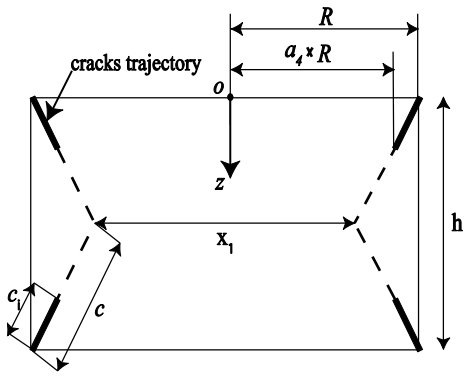

(b)

Fig.4 Illustration of idealized crack area parameters in unstrained state from rubber cylinder (adopted from Lindley and Stevenson 1981)

Based on that, the resulting internal crack length is calculated and represented as a function in terms of the position in radial direction, *r*, in the polar coordinate system as:

$$c(r) = -\left[\frac{(2K_1 r + K_2)}{4K_1} \sqrt{K_1 r^2 + K_2 r + K_3} + \frac{1}{2\sqrt{K_1}} \log\left(\frac{(K_2/2 + K_1 r)}{\sqrt{K_1}} + \sqrt{K_1 r^2 + K_2 r + K_3} \right) K_3 - \frac{1}{8K_1^{3/2}} \log\left(\frac{(K_2/2 + K_1 r)}{\sqrt{K_1}} + \sqrt{K_1 r^2 + K_2 r + K_3} \right) K_2^{\,2} \right] + C_1 \quad (12)$$

where K_1, K_2 and K_3 is from Eq. (13) through (15). In the fatigue failure mechanism of rubber bearing, internal cracks will initiate and propagate from the exterior edge of the laminate toward the center. Hence, C_1 can be determined by imposing the boundary condition $c(R) = 0$

$$K_1 = \left(2a_1 h / R^2\right)^2 \quad (13)$$

$$K_2 = 4a_1 a_2 h^2 / R^3 \quad (14)$$

$$K_3 = \left(a_2 h / R\right)^2 + 1 \quad (15)$$

Chou and Huang (2012) substituting Eq (11) into Eq. (8) – (10), all the stress components in the cylindrical coordinate system can be written as functions in terms of *r*, i.e. $\sigma_{rr}(r)$, $\sigma_{rz}(r)$, $\sigma_{\theta\theta}(r)$ and $\sigma_{rz}(r)$, the corresponding energy release rate *G*, cracks growth rate, *dc/dn*, crack length, *c*, in each intermediate fatigue stage, and the number of cycles *n* of circular rubber bearing subjected to cyclic compression can also be expressed as functions of *r* for each cracks propagation regime, i.e. $G(r)$. Accordingly, the number of cycles can be related to the energy release rate as follows:

Regime 1:

$$n = \int_{c_0}^{c_{G0}} \frac{dc}{\gamma} = \frac{c_{G0} - c_0}{\gamma} \tag{16}$$

Regime 2:

$$n = \int_{c_{G_0}}^{c_{G_t}} \frac{dc}{A(G(r) - G_0)} = \int_{r_{G_0}}^{r_{G_t}} A^{-1}[2\pi(1+\varepsilon_{p1}(r))^{-1/2} Wc(r)c(r) - G_0]^{-1} \times \sqrt{1 + \left(\frac{2a_1 h}{R^2} r + \frac{a_2 h}{R}\right)^2}\, dr \tag{17}$$

Regime 3:

$$n = \int_{c_{G_t}}^{c_{G_c}} a^{-1}\left[G(r)\right]^{-b} dc = \int_{r_{G_t}}^{r_{G_c}} a^{-1}\left[2\pi(1+\varepsilon_{p1}(r)^{-1/2} W_c(r)c(r)\right]^{-b} \times \sqrt{1 + \left(\frac{2a_1 h}{R^2} r + \frac{a_2 h}{R}\right)^2}\, dr \tag{18}$$

where c_{G0} and r_{G0} denote the crack length and r value at the state $G(r) = G_0$ respectively and γ is the crack growth rate in regime 1 which is assumed to be 5×10^{-4} cm/10^6 cycle.(Chou and Huang 2012)

Substituting Eq. (12) into Eq. (2) and (6), the change crack area, dA_c, internal stored energy change, dU, can be represented as a function of the position in the radial direction, r. That is, the number of cycles, n, of compressive loading is linked to the internal stored energy change, dU.

Chapter 3

Methodology

3.1 Analytical Model Formulation

Built on the existing knowledge and assumption, the relationship between the vertical stiffness of a degrading linear spring and the change in internal stored energy is developed and illustrated in Fig. 5.

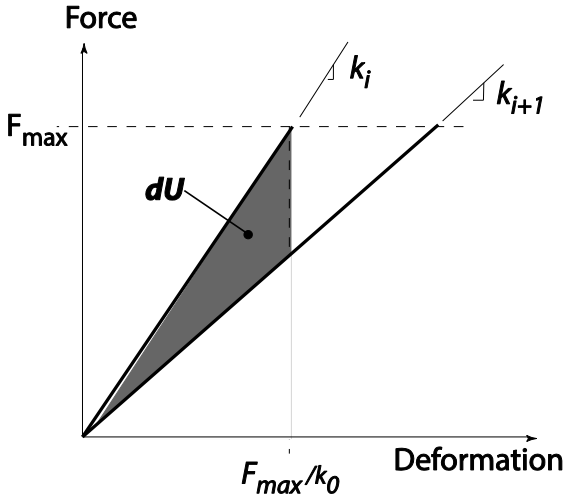

Fig. 5 Illustration of reducing stiffness for an elastomeric bearing with a linear force-displacement relationship under compressive loading

In Fig.5, k_i and k_{i+1} represent the vertical stiffness of an elastomeric bearing in intermediate fatigue stages, i and i+1 respectively. The energy released, dU, under subsequent cycles to a constant displacement is shown by the shaded region. From Fig. 4, the relationship between the vertical stiffness at i+1 cycles and the energy released can be expressed as:

$$k_{i+1} = \frac{2k_i^2}{F_{\max}^2}\left[dU(r_i) + \frac{F_{\max}^2}{2k_i} \right] \tag{19}$$

where and F_{max} is the maximum applied force equal to the maximum stress times the loaded area, A_b. Using Eq. (19) together with Eq. (2) through (18) a model has been developed to relate the stiffness of a bearing, k_i, to the number of cycles, n, of compressive loading. Because the stiffness at stage i+1 in Eq. (19) is related to the stiffness at stage i the simulation must begin with the initial stiffness for one layer of a solid circular elastomeric bearing, k_0, can be expressed as:

$$k_0 = \frac{\pi E_c R^2}{h} \tag{20}$$

where E_c is the compression modulus that is related to the shape factor of the bearing. For study the following compression modulus as presented in Horton et al. (2002) was adopted:

$$E_C = \frac{E}{1 - S\sqrt{\frac{2}{3}}\tanh\frac{1}{S}\sqrt{\frac{3}{2}}} \tag{21}$$

where E is the elastic modulus of the elastomer and S is the shape factor

3.2 Assumption

A number of assumptions are built into the analytical model as a result of the derivation of Eq. (19) and previous studies summarized by Eq. (2) through (18). These assumptions are:

1. The ratio of the minimum to maximum stress, "stress ratio," must be equal to zero which means the minimum stress must equal 0, If stress ratio is larger than zero, the strain crystallization mechanism at the crack tip will retard the crack growth rate within the rubber material so that Lake and Lindely's theory (1966) is no longer valid. There is currently no analytical model able to describe the energy release rate for stress ratios larger than zero;
2. The elastomer is assumed to be elastic and isotropic;
3. Deformations are sufficiently small to keep a liner relation between applied force and deformation and avoid breaking of the polymer chains or debonding of filler material;

4. The fatigue cracks are limited by a_4 to be sufficiently small as to not alter the stress distribution in the elastomer (Chou and Huang, 2012).
5. The principle stress controls the maximum strain energy density, W_c. That is, the cracks will initiate from the place with maximum strain energy density on the outmost of bonded rubber bearing, and then propagate along the lowest cracking energy density toward the center.

Equation (19) through (21) with Eq. (2) through (18) were combined to develop an analytical framework to simulate the stiffness degradation of a solid circular multilayered elastomeric bearing due to repeated cycles of compressive loading. The analytical framework as implemented in Matlab (MathWorks 2011) facilitates the simulation and sensitivity studies. The results of the simulation will allow the stiffness, *k*, to be plotted against cycles, *n*, from which the fatigue life and stiffness degradation can be determined. The analytical framework uses the parabolic function, *z/h*, in Eq. (11) to locate the crack position at the intermediate fatigue stage *i*, the energy release rate $G_{i,}$ cracks growth rate $(dc/dn)_i$, cracks length c_i, one cracked area A_{ci}, energy released, $dU_{i,}$ and stiffness k_i. Thus, at each fatigue stage from initial cycle until the crack no longer propagates, the cycles of loading, *n*, can be related to the vertical stiffness, *k*.

3.3 Sensitivity analysis

Sensitivity analysis quantifies how variability in a given model output can be attributed to variability in model factors (Saltelli et al. 2004). Sobol' method (Sobol' 1993), a global, variance based sensitivity analysis technique, is applied in this study. This method can be used to investigate the impact of any model factor (e.g. parameters, properties, and initial states) on model output if the factor uncertainty can be described probabilistically and the factors are statistically independent. Sobol' method has been previously utilized to diagnose other structural models (Arwade et al. 2010, Kala et al. 2011, Han et al. 2013). Though other sensitivity analyses exist, Sobol' method is regarded as a robust approach for a wide range of model complexities (Saltelli et al. 2008, Tang et al. 2007).

The Sobol' method quantifies sensitivity by partitioning the variance in model output into variance due to model factors. The total variance $V(y)$ in model output y can be written as

$$V(y) = \sum_i V_i + \sum_i \sum_{j>i} V_{ij} + ... + V_{12...m} \tag{22}$$

where m is the number of model factors; V_i is the variability of model output due to the ith factor; V_{ij} is the variability of output due to interaction of factors x_i and x_j; $V_{1,2,\ ...k}$ is the variability of output due to higher order interactions. The sensitivity of the output to a factor is quantified by a ratio of variance resulting in an index value ranging from 0 to 1. The "First order" Sobol sensitivity index used in this study denotes the effect of the ith factor alone and is determined according to:

$$S_i = \frac{V_i}{V(y)} \tag{23}$$

The "total order" Sobol sensitivity index reflects the effect of the ith factor and the interactions between the ith factors and other factors and is determined according to:

$$S_{Ti} = 1 - \frac{V_{\sim i}}{V(y)} \tag{24}$$

where $V_{\sim i}$ is the variance from all factors but ith. In other words, the total order index S_{Ti} is the sum of the interactions index with factor i and the first order index S_i.

In this study two quantities are used to describe the model output, specifically the fatigue life, n_f, and stiffness degradation, D_s, as illustrated in Fig. 1.The model factors considered for the sensitivity study are c_0, g_0, A, g_t, a, b, a_2, a_4, and E. The range of values material parameters, c_0, g_0, A, g_t, a and b were based test results from Chou and Huang (2012). The elastic modulus, E, was varied from 2 MPa to 40 MPa in an attempt to understand the impact of material selection since the type of material used in elastomeric bearings varies widely from one application to another.

Table 2 Range of the material parameters in sensitivity analysis

No.	Factor	Name	Range		Unit
			Lower	Upper	
1	c_0	Initial flaws	11.06	105.71	μm
2	G_0	Threshold 1	0.048	0.239	KJ/m^2
3	A	Material Parameter	0.21	1.66	NA
4	G_t	Threshold 2	0.33	0.61	KJ/m^2
5	a	Material Parameter	1.74	104.62	NA
6	b	Material Parameter	3.19	6.05	NA
7	E	Elastic modulus	2	40	MPa
8	a_2	Trajectory parameters	133.6*	139.8*	NA
9	a_4	Trajectory parameters	0.96*	0.969*	NA

*denotes the upper and lower limit of the cracks trajectory parameters a_2, a_4 for the shape factor S=2.5

To investigate the sensitivity of the model output to variations in the crack path, the crack trajectory was varied. However the crack path is dependent on parameters a_1, a_2, and a_3 so that they could not all be varied simultaneously. Therefore to vary the crack trajectory in a systematic manner, parameter a_1 was specified by the shape factor S while a_3= -a_1-a_2 to satisfy the condition that $z/h(1)$=0, i.e., the longitudinal direction of the crack is equal to zero at the outmost of bonded rubber layer (r/R)=1 . The range of a_2 and a_4 are decided by ensuring Eq. (11) is monotonic and its maximum value is smaller than 0.5 in the region -a_2/2/a_1<r/R<1. The material and trajectory factors are listed in Tables 2 and 3 along with the corresponding range values.

Table 3. Range of the trajectory parameters in sensitivity analysis

Shape Factor S	a_1	a_2		a_4	
		Lower	Upper	Lower	Upper
2.5	-72.835	133.6	139.8	0.96	0.969
5	-264.53	506.1	518.5	0.98	0.989
10	-1022.6	2000.0	2024.7	0.99	0.999
20	-3935.3	7781.9	7791.9	0.99	0.999

The sensitivity study was performed for a set of parameter scenarios. Specifically the sensitivity analysis was repeated for combinations of shape factors, *S*, ranging from 2.5 to 20 and maximum stress, σ_{max}, ranging from 2.5 MPa to 10 MPa so that a total of 24 sets of sensitivity indices were generated with the model output from the simulation model.

3.4 Numerical simulation and model evaluation

The results of the numerical simulation for circular EPDM rubber bearing with shape factor 5 and elastic modulus 2 MPa subjected to maximum applied stress 10 MPa are plotted in Fig. 6. The horizontal axis is the number of cycles of loading, *n*, and the vertical axis is the compressive stiffness, k_i, after *n* cycles of loading normalized by the initial compressive stiffness, k_o. As other material types, e.g. steel, the stiffness degradation of rubber starts from a slow initiation and through a dramatically decreasing approaching a stabilized value. Fig. 6 is annotated to show the model output in which the stiffness degradation equals -13.5% after 1.56×10^4 number of cycles while the time taken for dramatically stiffness decreasing is 40.4. Roeder et al. (1990) reported a 18.9% stiffness degradation after the same number of cycles for square chloroprene rubber bearing with the same shape factor say 5 but subjected to different

applied stress range 0.8-10.4MPa. The fatigue life estimate from the simulation could not be evaluated because Roeder et al. did not provide stiffness degradation data throughout the test. Qualitatively comparison between stiffness degradation under the same number of cycles of simulation and Roeder experiment data say 13.5% to 18.9% does e suggest the results from the analytical model are reasonable in that the magnitude of the stiffness degradation is on the same order as that determined from the test.

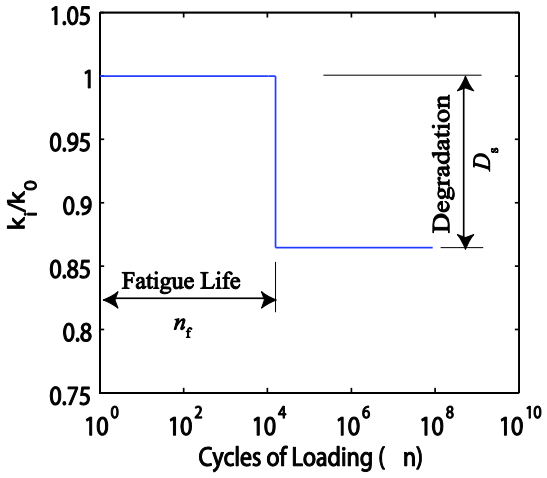

Fig. 6 Results of simulation for shape factor S= 5, elastic modulus E= 2MPa and Maximum compressive stress σ_{max}=10MPa

3.5 Parametric and sensitivity analyses

3.5.1 Parametric analysis

Parametric and sensitivity analyses were performed to understand the effect of loading, bearing geometry, bearing material and model parameter variability on the model output, specifically, the estimated stiffness degradation and fatigue life. Figure presents simulation results for solid circular bearings with shape factors, *S*, ranging from 2.5 to 20 and elastic modulus, *E*, ranging from 2 MPa to 40 MPa with a maximum compressive stress, σ_{max}, of 10 MPa. Two trends are apparent from the results presented in Fig. 7, specifically as the shape factor decreases the stiffness degradation at the end of the

fatigue life increases and for a given shape factor as the elastic modulus decreases the fatigue life decreases.

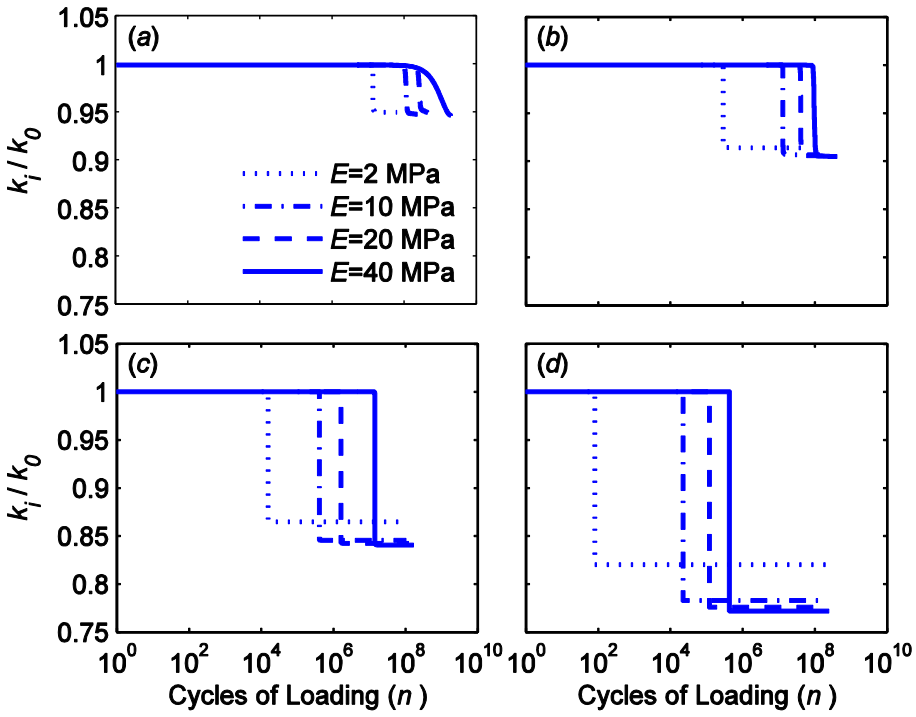

Fig. 7 Results from simulation of elastomeric bearings subjected to cyclic loading with a maximum stress equal 10 MPa and shape factors of: (a) S=20 (b) S=10 (c) S=5 (d) S=2.5

For a bearing with S=2.5, E=10MPa, and σ_{max}=10 MPa a 21.7% reduction in stiffness is estimated after 2.25×10^4 cycles of loading. Figure 8, presents the results from simulation performed with a σ_{max}=5 MPa for the same shape factors and elastic modulus as in Fig. 7. The results in Fig. 8 show similar trends in that as the shape factor decreases the stiffness degradation increases and for a given shape factor as the elastic modulus decreases the fatigue life decreases. For a bearing with S=2.5, E=10 MPa, and σ_{max}=5 MPa a 21.9% reduction in stiffness is estimated after 4.7×10^5 cycles of loading. Comparing this to case with σ_{max}=10 MPa (Fig.7d) suggests the peak compressive stress does not significantly affect the stiffness degradation however reducing the peak compressive stress increases the fatigue life.

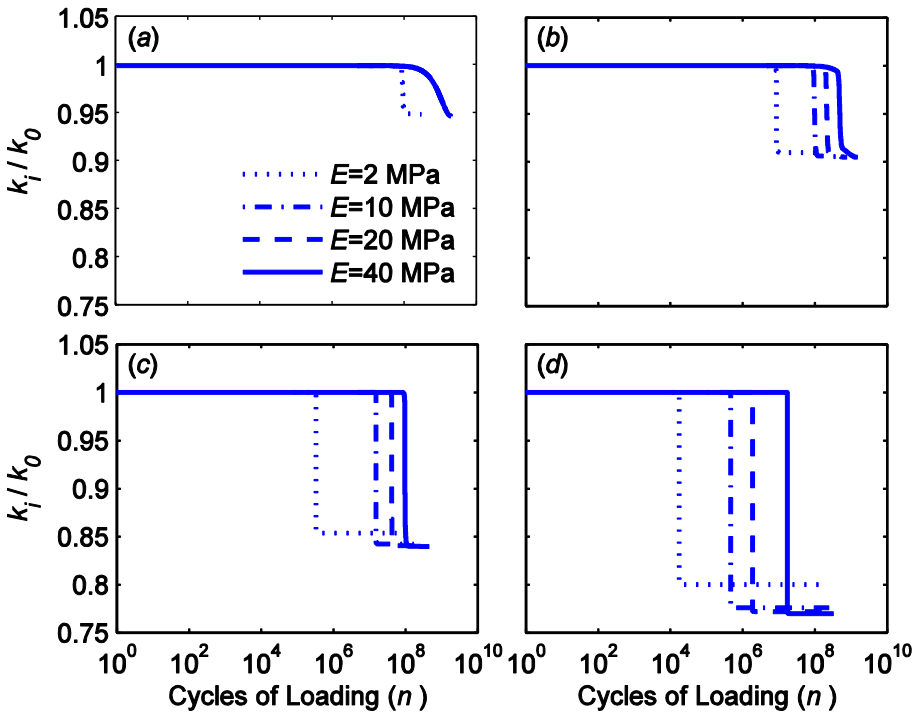

Fig. 8 Results from simulation of elastomeric bearings subjected to cyclic loading with a maximum stress equal 5 MPa and shape factors of: (a) S=20 (b) S=10 (c) S=5 (d) S=2.5

Figure 9 presents simulation results for σ_{max}=2.5 MPa. Again the trends are similar to those observed in Figs. 7 and 8. For a bearing with S=2.5, E=10MPa, and σ_{max}=2.5 MPa a 22% reduction in stiffness is estimated after 1.7×10^7 cycles of loading again suggesting that as the maximum compressive stress is reduced the fatigue life increases.

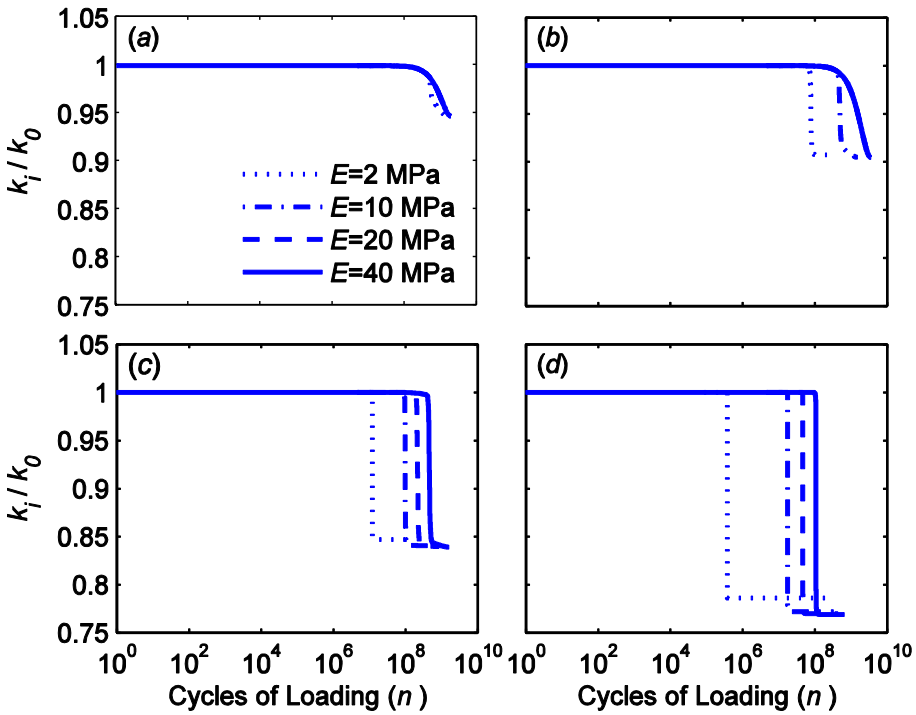

Fig. 9 Results from simulation of elastomeric bearings subjected to cyclic loading with a maximum stress equal 2.5 MPa and shape factors of: (a) S=20 (b) S=10 (c) S=5 (d) S=2.5

The influence of the elastic modulus, maximum compressive stress and shape factor is summarized in Fig.10 and Fig 11. It is summarized an increased elastic modulus E will result the fatigue life and stiffness degradation increasing correspondingly while the maximum compressive stress has the opposite effect. A larger shape factor will lead a longer fatigue life and smaller stiffness degradation suggesting larger shape factor gives a better fatigue resistance.

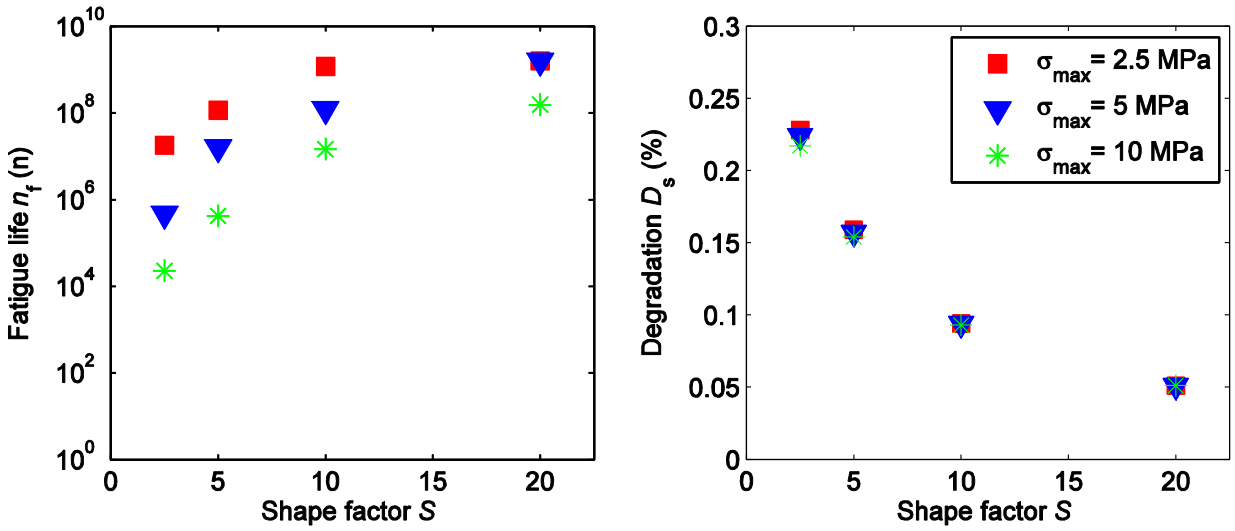

Fig. 10 Fatigue life and degradation for elastic modulus E=10 MPa rubber bearings with different shape factors and subjected to different applied load

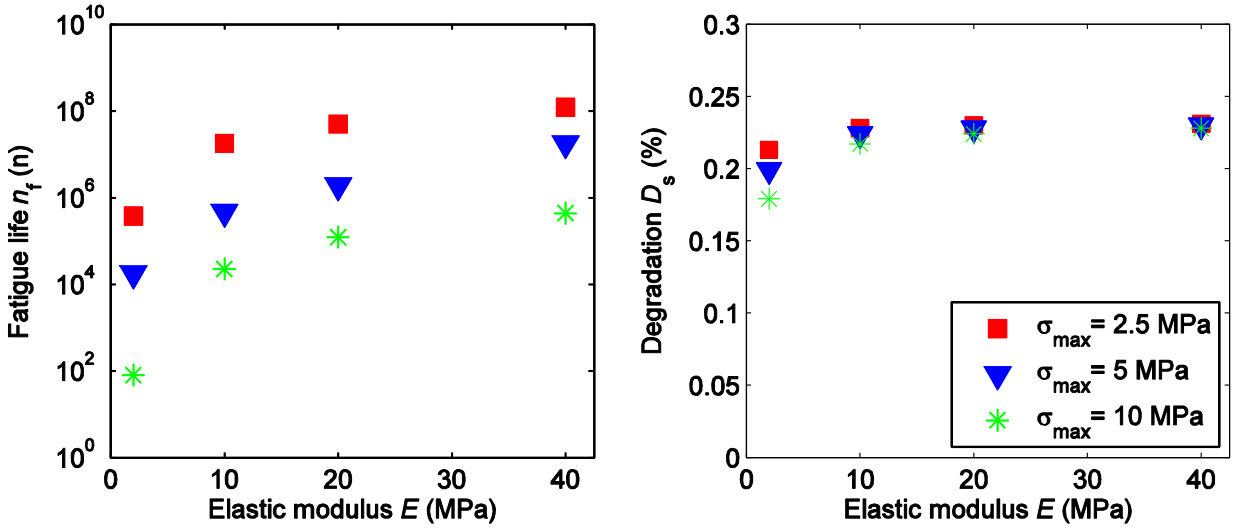

Fig. 11 Fatigue life and degradation for shape factor S=2.5 rubber bearings with different elastic modulus and subjected to different applied load

3.5.2 Sensitivity analysis

Sobol's method was applied to the output from the analytical model, specifically the stiffness degradation D_s and fatigue life n_f, to compute sensitivity indices for the nine independent model factors c_0, g_0, A, g_t, a, b, a_2, a_3, and E to identify the relative importance of the individual model factors for simulating the stiffness degradation and fatigue life. The sensitivity analysis was performed on an ensemble of fatigue life and stiffness degradation data for twelve sets of S and σ_{max}. The model factors and factor numbers along with the range of values for each factor are presented in Table 2. Each parameter was assumed to be uniformly distributed over the range presented in Table 2.

Sensitivity indices for each model factor corresponding to stiffness degradation are presented in Fig. 12 for each of the twelve combinations of S and σ_{max}. Each plot presents the first order, S_1, second order, e.g. $S_{2,1}$ and higher order, S_h, sensitivity indices for each factor. For the second order index, the first subscript number denotes the order of the sensitivity index and the second the factors in which there is interaction. For a specific factor, the sum of the first order, second and higher order indices equals the total sensitivity index presented in Eq. (24). From the results presented in Fig. 12, for S=2.5, the estimated stiffness degradation is most sensitive to factors 7, 8 and 9 that correspond to E, a_2 and a_4. This suggests that the elastic modulus and the crack path, Eq. (11) are the most important factors for estimating the stiffness reduction. As the shape factor increases, the stiffness degradation is increasingly sensitive only to factor 9, i.e. a_4,that represents the position along the radial direction in which the crack is stopped. This results suggest that for low shape factors bearings, i.e. S=2.5 the fatigue cracks are self limiting and that imposing a restriction on the crack propagation does not affect the simulated stiffness degradation. In contrast for large shape factors, i.e. S=20 the crack might not be self limiting and that the crack propagation should not be restricted. Relaxing the restriction imposed by a_4 would require a through investigation of whether the assumption that the stress distribution is unaffected by the presence of the crack, assumption No. 4, is valid. However this is beyond the scope of the current work as it would require detailed finite element or continuum modeling to update the stress values as the crack propagates through the elastomer.

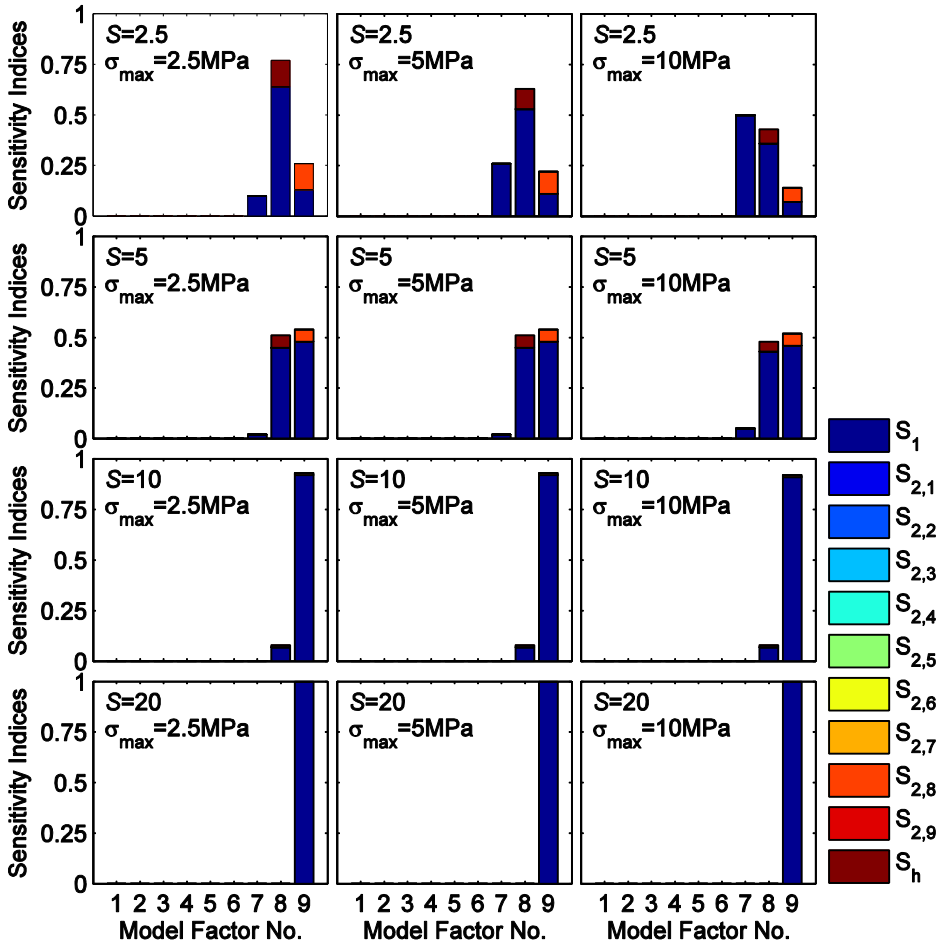

Fig. 12 Sobol's sensitivity indices for stiffness degradation

Figure 13 presents sensitivity indices corresponding to the fatigue life for the nine model factors and the twelve parameter sets. From Fig. 13, for lower shape factors, i.e. S=2.5 and 5, the estimated fatigue life is most sensitive to factors 2 and 7 corresponding to c_o and E that are material parameters related to the intrinsic flaws and the elastic modulus. For larger shape factors, i.e. 10 and 20, there is more sensitivity again to factors 8 and 9 (a_2 and a_4) corresponding to the crack path.

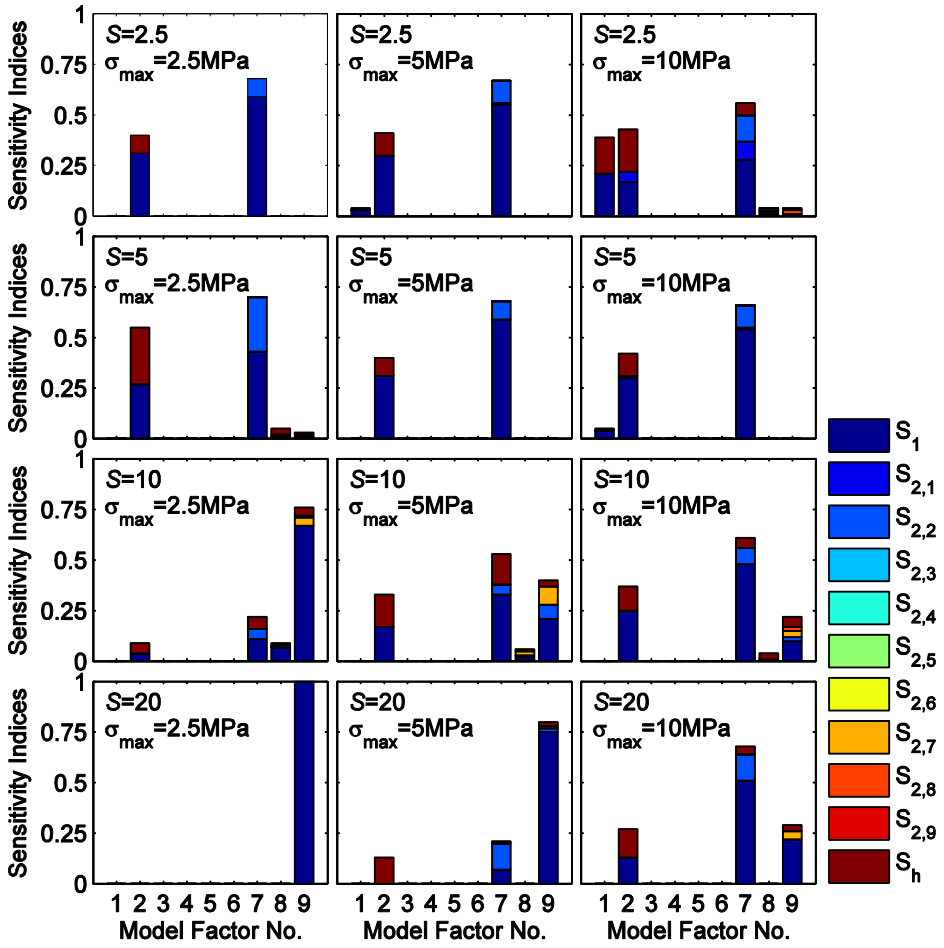

Fig. 13 Sobol's sensitivity indices for fatigue life

Chapter 4

Conclusions

An analytical model for simulating the compression stiffness degradation in solid circular elastomeric bearings subjected to cyclic compressive loading has been developed. The model builds on work of others from past studies (Rivlin and Thomas 1953; Lindely and Stevenson 1981; Chou and Huang 2012) to link the number of cycles of compressive loading to a reduced stiffness through the energy released by the propagation of fatigue cracks in the elastomer. The model is limited to solid circular bearings subjected to cyclic compressive loading with a stress ratio equal to zero meaning bearing is fully relaxed in each cyclic loading. Furthermore the model assumes linear force-displacement relationship and a number of other assumptions adopted from previous work.

A qualitative comparison of the results of model simulation with experimental tests performed by Roeder et al. (1990) suggest the stiffness degradation estimated with the analytical model agrees reasonably well with that determined from experimental testing. Unfortunately, the limited fatigue data available for elastomeric bearings precluded a more rigorous evaluation of the analytical model.

While the versatility of the model is limited at this point by a number of assumptions, the results of the parametric simulations provided useful insight about the effect loading, bearing geometry and bearing material have on both the stiffness degradation and fatigue life of elastomeric bearings. Furthermore, a global variance-based sensitivity analysis was performed on ensembles of the model output to gain insight as to how variability in the model factors affect the estimated stiffness degradation and fatigue life from the model simulation. Based on the results of the parametric and sensitivity analyzes the following conclusion are drawn:

- The stiffness degradation in elastomeric bearings with low shape factors is significant suggesting the stiffness properties of bridge bearings with shape factors ranging from 3-5 could reduce by 20 to 30% over their service life. This level of reduction in stiffness in the supporting elements could

translated into importance changes in the dynamic behavior of the bridge and/or be captures in global monitoring systems. On the contrary, the degradation of large shape factors say 20 is as small as 5%.

- The increasing shape factor will result in a longer fatigue life but smaller stiffness degradation which enhances the vertical fatigue resistance of the circular elastomeric bearing can be adopted for rubber fatigue design. However, it is not reasonable to increase the fatigue resistance by solely increasing the elastic modulus which can extend the fatigue life but also severe the stiffness degradation.
- The fatigue life is sensitive to the trajectory of the crack path, i.e. a_2 and the radial location where the crack propagation is limited, a_4 and material factors, i.e. initial cracks length, c_0, energy release rate G_0 and elastic modulus E. For small maximum applied stress say σ_{max}=2.5 MPa, the total sensitivity indices of a_4 which represents the importance of the limitation of cracks trajectory for the fatigue life increases from 0 to 1with increasing shape factor from 2.5 to 20.
- The stiffness degradation is sensitive to the elastic modulus E and in addition to the crack trajectory factors, i.e. a_2 and a_4. The sensitivity of the material parameters E decreases with decreasing maximum compressive stress and increasing shape factor, e.g. for maximum applied stress σ_{max}=2.5 MPa, the total sensitivity indices of elastic modulus E decreases from 0.1 to 0 when shape factor increases from 2.5 to 20. The sensitivity to a_4 increases with an increased shape factor, e.g. for maximum applied stress σ_{max}=2.5 MPa, the total sensitivity indices of a_4 ranges from 0.26 to 1 when shape factor increases from 2.5 to 20, suggesting that for larger shape factor bearings the crack propagation should not be limited and that the assumption that the crack does not affect alter the stress distribution should be investigate further in an attempt to relax this constraint;

References

AASHTO (1999), Guide specifications for seismic isolation design, AASHTO, Washington, D.C.

Arwade, S. R., Moradi, M., and Louhghalam, A. (2010), "Variance decomposition and global sensitivity 22 for structural systems." *Eng. Struct.*, 32(1), 1–10.

National Bridge Inventory (no date), "Bridge Statistics for Pittsburgh, Pennsylvania (PA) – Condition, Traffic, Stress, Structural Evaluation, Project Costs". *City-Data* <http://www.city-data.com/bridges/bridges-Pittsburgh-Pennsylvania.html> (May 5,2013)

Chou, H. W. and Huang, J. S. (2012), "Fatigue life prediction for circular rubber bearings subjected to cyclic compression*". J. Appl. Polym. Sci*., 123, 2194-2203

Chou, H. W. and Huang, J. S. (2011), "Crack initiation and propagation in circular rubber bearings subjected to cyclic compression". *J. Appl. Polym. Sci*., 121, 1747-1756

Chou, H. W. and Huang, J. S. (2008), "Effects of cyclic compression and thermal aging on dynamic properties of neoprene rubber bearings". *J. Appl. Polym. Sci*., 107, 1635-1641

Chou, H. W. and Huang, J. S. (2007), "Effects of thermal aging on fatigue of carbon black–reinforced EPDM rubber". *J. Appl. Polym. Sci*., 103, 1244-1251

Gent, A. N. and Lindley, P. B. (1959), "The compression of bonded rubber blocks." *Proc., Inst. Mech. Eng*., 173, 111-122

Han, X, Kelleher, C. A. and Warn, G.P. (2013), "Identification of the controlling mechanism for predicting critical loads in elastomeric bearings." *J. Struct. Eng.*, doi:10.1061/(ASCE)ST.1943-541X.0000811

Horton, J. M., Tupholme, G. E. and Gover, M. J. C. (2002), "Axial loading of bonded rubber blocks". ASME *J. Appl. Mech*., 69, 836-834

Kala, Z. (2011), "Sensitivity analysis of steel plane frames with initial imperfections." *Eng. Struct*., 33(8), 21 2342–2349.

Lake, G. J. and Lindley, P. B. (1966), "Fatigue of rubber at low strains", *J. Appl. Polym. Sci*., 10, 343-351

Lake, G. J. (2003), "Fracture mechanics and its application to failure in rubber articles". *Rubber Chem. Technol*., 76, 567-591

Lindley, P. B. and Stevenson, A. (1981), "Fatigue resistance of natural rubber in compression". *Proc. Mater*. Exp. Design Fatigue. 55, 337-351

Lindley, P. B. (1972), "Energy for crack growth in model rubber components", *J. Strain Anal.* 7, 132-140

MathWorks (2011), *Matlab Version 7.11.0584*, The MathWorks, Inc., Natick, MA.

Mars, W. V. and Fatemi, A. (2001), "A literature Survey on fatigue analysis approaches for rubber". *Int. J. Fatigue*, 24, 949–961

Mars, W. V (2002), "Cracking energy density as a predictor of fatigue life under multiaxial conditions". *Rubber chem. Technol*, 75 , 1-17

Riviln, R. S. and Thomas, A. G. (1953), "Rupture of rubber. I. characteristic energy for tearing." *J. Polym. Sci*, 10, 291-318,

Roeder, C. W., Stanton, J. F. and Taylor, A. W. (1990), "Fatigue of steel-reinforced elastomeric bearings". *J. Strl. Engrg*., 116, 407-426

Saltelli, A., Tarantola, S., Campolongo, F., and Ratto, M. (2004), *Sensitivity Analysis in Practice: A guide to assessing scientific models*, Wiley, Hoboken, NJ.

Saltelli, A., Ratto, M., Andres, T., Campolongo, T., Cariboni, J., Gatelli, D., Saisana, M., and Tarantola, S. (2008), *Global sensitivity analysis: the primer*, Wiley, Hoboken, NJ.

Simlab (2011), Software package for uncertainty and sensitivity analysis. Joint Research Centre of the European Commission. Downloadable for free at:http://simlab.jrc.ec.europa.eu.

Sobol', I. M. (1967), "On the distribution of points in a cube and the approximate evaluation of integrals." *USSR Computational Mathematics and Mathematical Physics*, 7(4), 784–802.

Sobol', I. M. (1990), "Sensitivity estimates for nonlinear mathematical models." *Matematicheskoe Modelirovanie*, 2(1), 112–118. In Russian, translated in English in Sobol' (1993).

Sobol', I. M. (1993), "Sensitivity analysis for non-linear mathematical models." *Mathematical Modelling and Computational Experiment*, 1(4), 407–414. English translation of Russian original paper, Sobol' (1990).

Sobol', I. M. (2001), "Global sensitivity indices for nonlinear mathematical models and their Monte Carlo estimates." *Mathematics and Computers in Simulation*, 55(1-3), 271–280.

Tang, Y., Reed, P., Wagener, T., and van Werkhoven, K. (2007), "Comparing sensitivity analysis methods to advance lumped watershed model identification and evaluation." *Hydrol Earth SystSci*, 2611(2), 793–817.

Thomas A. G. (1958), "Rupture of rubber. V. Cut growth in natural rubber vulcanizates". *J. Polym. Sci*. 31, 467–80.

Appendix

Energy and Principal Stress Calculation

Under the cylindrical coordinate system, the stress at one particular point, σ_{rr}, σ_{zz} and σ_{rz} can be transformed into two principal stresses σ_{P1} and σ_{P2} easily by Mohr's Circle as showed in Fig. 14.

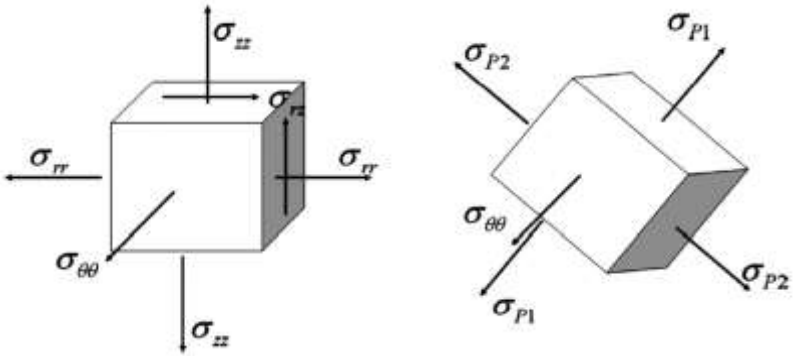

Figure 14. Stresses and transformed from cylindrical coordinate to principal coordinate on the γ-z plane (adopted from Chou and Huang 2012)

As for the stress components, σ_{rr}, σ_{rz}, $\sigma_{\theta\theta}$, the expressions quoted from Horton et al. (2002) can be used here to represent them [equation (8), (9) and (10) in Chapter 2]. All the factors in these stress expressions are arbitrary values except for *z* which is the depth of the cracks in the cylinder. The function of *z* is synthesized to describe the geometry of cracks by Chou and Huang (2012) sated in equation (11). Thus the principal stresses at one certain point could be obtained in terms of the position of this point in the cross section, *r*, representing as follows.

$$\sigma_{p1} = \frac{(\sigma_{rr} + \sigma_{zz})}{2} + \frac{\sqrt{(\sigma_{rr} - \sigma_{zz})^2 + (2\sigma_{rz})^2}}{2} \tag{25}$$

$$\sigma_{p2} = \frac{(\sigma_{rr} + \sigma_{zz})}{2} - \frac{\sqrt{(\sigma_{rr} - \sigma_{zz})^2 + (2\sigma_{rz})^2}}{2} \tag{26}$$

As for the maximum cracking energy density, W_c, at the crack position, one thing should be ensured before calculation is the maximum principal stress σ_{P1} must always be larger than zero because cracks initiation is due to the largest tension stress at this point. At any point, W_c is calculated using*:*

$$W_c = \frac{\sigma \cdot \varepsilon}{2} = \frac{\sigma_{p1} \cdot (\sigma_{p1} - \nu\sigma_{p2} - \nu\sigma_{\theta\theta})}{2E} = \frac{1}{2E}(\sigma_{p1}{}^2 - \nu\sigma_{p1}\sigma_{p2} - \nu\sigma_{p1}\sigma_{\theta\theta}) \tag{27}$$

Where υ is position ratio, approximately equaling 0.5 and E is the young's modulus of rubber material.